Electronic Supplementary Information

Effect of molecular ordering on circularly polarized emission from twisted mesogenic conjugated polymer

Dong-Min Lee, Gi-Eun Kim, Jae-Hoon Kim * and Chang-Jae Yu *

Department of Electronic Engineering, Hanyang University, Seoul 04763, Korea.

**E-mail: jhoon@hanyang.ac.kr, cjyu@hanyang.ac.kr*

1. Light efficiency of OLED depending on direct emission of circularly polarized light

In a conventional OLED for display applications, a circular polarizer is needed to prevent reflection of ambient light from a metal cathode. However, use of a circular polarizer can only result in extraction of half the emitted light from an OLED panel. Therefore, the maximum efficiency of the light emitted is 50 % at best, even without considering other losses such as internal reflection and absorption in the OLED stacks. Direct emission of circularly polarized (CP) light from the emitting layer in OLED devices can therefore increase the light efficiency without any other functional structure. The degree of CP light is defined by the dissymmetry factor, $g = 2\,(I_L - I_R)/(I_L + I_R)$, where I_L and I_R indicate the intensities of left-handed and right-handed CP emission, respectively

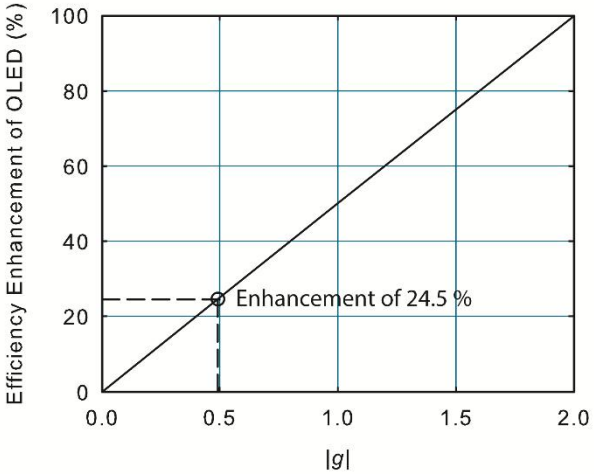

Fig. S1 Efficiency enhancement of OLED as a function of g value.

The factor g has a value between +2 and -2. The zero g value indicates a light component without any circular polarization, whereas +2 and −2 correspond to fully I_L and I_R, respectively. Also, I_R is expressed by the g value, $I_R = (2 + g)/4$, because sum of I_L and I_R is unity when total intensity is normalized. Therefore, a ratio of the efficiency enhancement of OLED under a circular polarizer can be represented by

$$\eta = \frac{g}{2} \times 100\ (\%)$$

The maximum g value of 0.49 measured here for EL is applied to OLEDs to improve the light efficiency by 24.5 % compared to non-polarized conventional OLEDs that use a common circular polarizer as shown in Fig. S1.

2. DSC data of the F8BT

The phase transition temperature of the F8BT was determined by differential scanning calorimeter (DSC 200 F3, NETZSCH) performed in a nitrogen atmosphere with heating rates of 10 °C/min as shown in Fig. S2. The transition temperature was observed at about 135 °C. Also, several literatures[1,2] reported the transition temperature of the F8BT to be about 130 °C. As a result, the annealing temperature of 160 °C used here is suitable for generation of the twist structure of the F8BT by the chiral dopant.

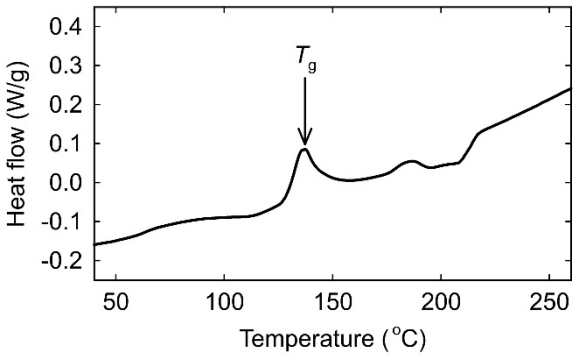

Fig. S2 DSC data of the F8BT with heating rates of 10 °C/min. The transition temperature is observed at about 135 °C.

3. Order parameter and birefringence of the samples with various contact distances

According to a contact distance, the order parameter and the birefringence were estimated by measurement of the LPPL spectra under polarisers parallel and perpendicular to the rubbing direction, and measurement of the phase retardation with respect to the sample-rotating angle,[3] respectively. From the LPPL spectra measured under polarisers parallel ($I_{\parallel}$) and perpendicular ($I_{\perp}$) to the rubbing direction, the polarization ratio (R_P) of the LP light is expressed as an intensity ratio of the parallel component to the perpendicular one of LP light ($R_P = I_{\parallel}/I_{\perp}$) and the corresponding order parameter is written as $S = (R_P - 1)/(R_P + 2)$.[4] Here, intensities of the parallel and the perpendicular component were determined at 546 nm.

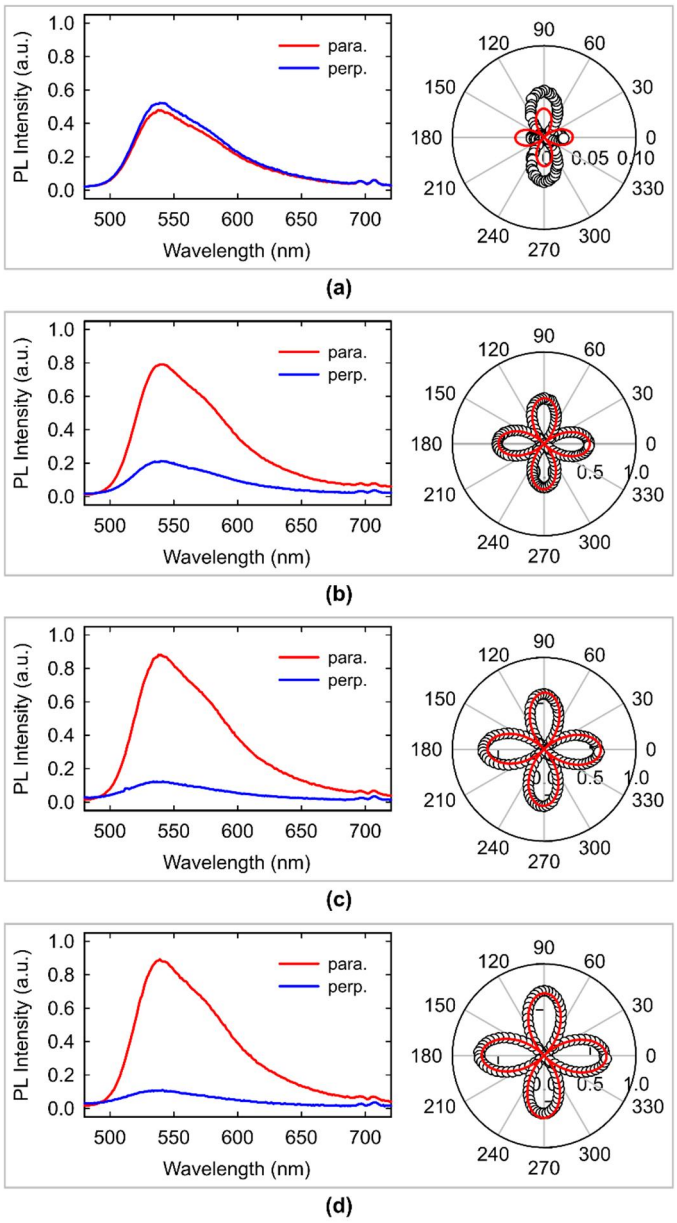

Fig. S3 The LPPL spectra and the phase retardation of the 100-nm-thick F8BT films without chiral dopant on the rubbed alignment layer with contact distance of (a) 0, (b) 10, (c) 20, and (d) 30 μm. The spectra (left figures) were measured under linear polarizer, both parallel (red solid curve) and perpendicular (blue solid curve) to the rubbing direction. The measured phase retardation (symbols) of the samples as a function of rotation angle using PEM method (right figures). The least-square-fits of the retardation are depicted by red solid line.

To evaluate the birefringence, we used the phase modulation technique by a photoelastic modulator (PEM) has been used. Although this method has already been expressed in detail at ESI in Ref. 5, we describe whole procedure again. The PEM generates the time-dependent phase shift $A(t) = A_0 \cos(\omega t)$ with an amplitude A_0 and a frequency ω. Suppose that B depicts the phase retardation of a sample at a certain rotation angle θ with respect to the optic axis of the PEM under crossed polarizers, the transmitted intensity through the sample and the PEM is

$$E = \frac{1}{2}(1 \quad -1)\begin{pmatrix} \exp\left[i\frac{B}{2}\right] & 0 \\ 0 & \exp\left[-i\frac{B}{2}\right] \end{pmatrix}\begin{pmatrix} \exp\left[i\frac{A_0}{2}\cos(\omega t)\right] & 0 \\ 0 & \exp\left[-i\frac{A_0}{2}\cos(\omega t)\right] \end{pmatrix}\begin{pmatrix} 1 \\ 1 \end{pmatrix}$$

$$I = E^*E = \frac{1}{2}\{1 - J_0(A_0)\cos B\} + \frac{1}{2}J_1(A_0)\sin B\cos(\omega t) + \frac{1}{2}J_2(A_0)\cos B\cos(2\omega t) + \cdots$$

where $J_0(A_0)$, $J_1(A_0)$, and $J_2(A_0)$ denote the zeroth, first and second orders of the Bessel function, respectively. To eliminate the dependence of phase retardation B in the zeroth harmonics, we determine the modulation amplitude A_0 so that $J_0(A_0) = 0$. By using a lock-in amplifier, we can measure the intensities I_1 and I_2 of the first and the second harmonic terms, respectively.

$$I_1 = \frac{1}{2} J_1(A_0) \sin(B)$$

$$I_2 = \frac{1}{2} J_2(A_0) \cos(B)$$

Finally, we can determine the phase retardation B as rotating the sample (rotation angle θ) following as,

$$B(\theta) = \tan^{-1}\left(\frac{J_2 I_1}{J_1 I_2}\right)$$

As a result, for a given angle θ, we have measured the $B(\theta)$ as shown in Fig. 2(a). Now, to determine the phase retardation B_0 of the sample, which is a maximum $B(\theta)$ at $\theta = 0$ (when the optic axis is parallel to that of the PEM), the transmitted intensity is modified as

$$E = \frac{1}{2}\begin{pmatrix}1 & -1\end{pmatrix}\begin{pmatrix}\cos\theta & -\sin\theta \\ \sin\theta & \cos\theta\end{pmatrix}\begin{pmatrix}e^{i\frac{B_0}{2}} & 0 \\ 0 & e^{-i\frac{B_0}{2}}\end{pmatrix}\begin{pmatrix}\cos\theta & \sin\theta \\ -\sin\theta & \cos\theta\end{pmatrix}\begin{pmatrix}\exp\left[i\frac{A_0}{2}\cos(\omega t)\right] & 0 \\ 0 & \exp\left[-i\frac{A_0}{2}\cos(\omega t)\right]\end{pmatrix}\begin{pmatrix}1 \\ 1\end{pmatrix}$$

$$I = E^* E = I_{dc} + J_1(A_0)\sin B_0 \cos(2\theta)\cos(\omega t) + \frac{1}{2} J_2(A_0)[1 - \cos(4\theta) + \{1 + \cos(4\theta)\}\cos B_0]\cos(2\omega t) + \cdots$$

Here, I_{dc} denotes the dc component of the transmitted intensity. For fitting the phase retardation B_0, we can use the following equation after comparing the above $B(\theta)$[1]

$$B(\theta) = \tan^{-1}\left[\frac{2\sin B_0 \cos(2\theta)}{1 - \cos(4\theta) + \{1 + \cos(4\theta)\}\cos B_0}\right]$$

For the samples prepared with various contact distances, the LPPL spectra under polarisers parallel and perpendicular to the rubbing direction and the $B(\theta)$ values were measured as shown in Fig. S3.

4. Evaluation of total twisted angle as a function of blending concentration of chiral dopant

For evaluation of total twist angle of the F8BT with chiral dopant layer with 100 nm thickness, we used the Mueller matrix analysis incorporating the Stokes parameter.[6] We divided the F8BT layer into 10 sublayers of 10 nm and assumed that the layer rotates continuously and uniformly. The twisted angle of the *i*-th sublayer is expressed as $\theta_i = \theta_T(z_i/d)$, where θ_T, z_i, and d denote the total twisted angle, distance from the hole blocking layer, and the film thickness, respectively. Then, the theoretical Stokes parameters using Mueller matrix and after passing through the F8BT layer twisted to θ_T are compared to the measured parameters as shown in Fig. S4. All measured Stokes parameters are represented by horizontal black lines, and theoretically calculated parameters are represented by open circles.

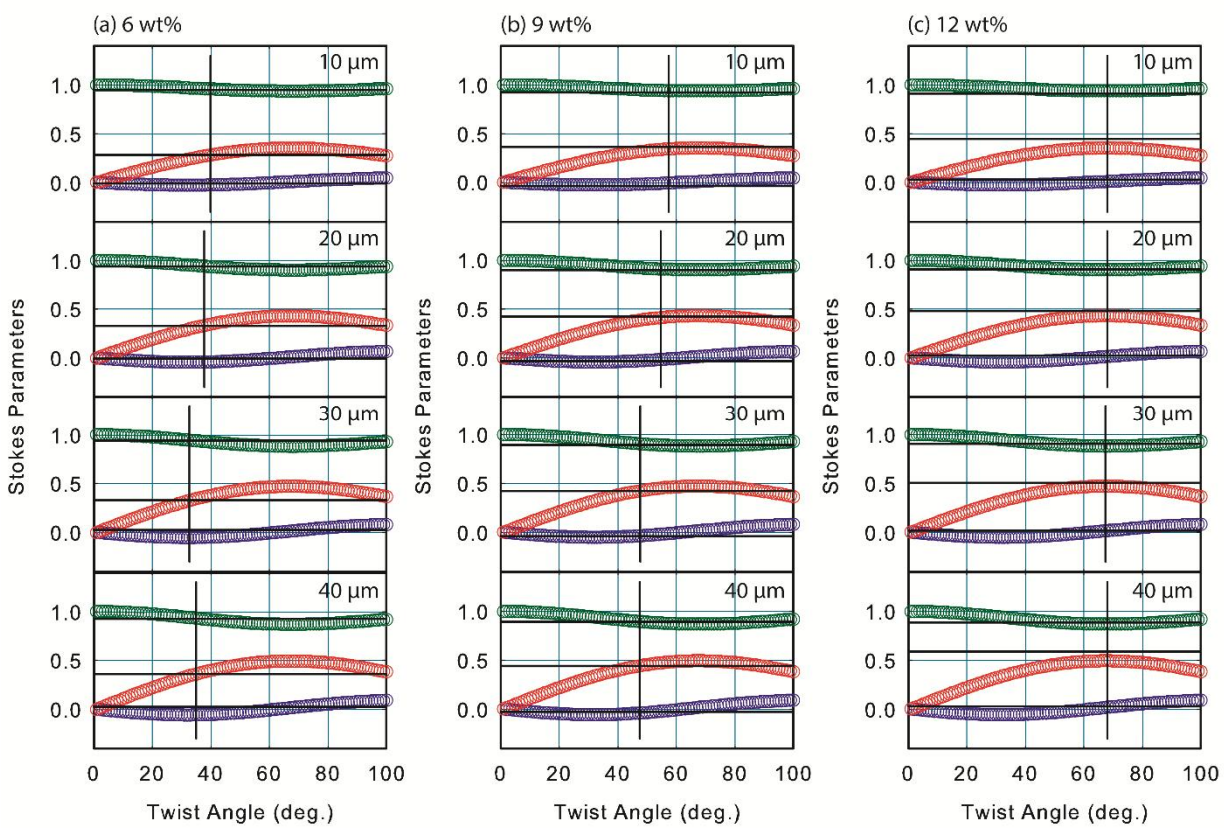

Figure S4. The measured Stokes parameters (horizontal black lines), theoretically derived parameters (open circles), and the corresponding least-squares-fit (vertical lines). The Stokes parameters were measured depending on blending concentration of chiral dopant (6, 9, and 12 wt%) from samples fabricated by controlling the contact distance from 10 to 40 μm.

The chiral dopant, R5011, with high helical twisting power (HTP) forms a helical conformation of mesogenic polymer. The helical pitch of the twisted layer is inversely proportional to the blending concentration of the chiral dopant and represented as $p = 1/(HTP \times c)$, where p and c are the pitch of the twisted stacking and concentration of the chiral dopant, respectively.[7] The twisted angle is expressed as $\theta_T = 2\pi d(HTP \times c)$ for a given thickness (d) of the F8BT layer. Therefore, the twisted angles have values within a certain range and increase consistently depending only on blending concentration of the chiral dopant regardless of molecular ordering (Fig. S5). Moreover, the 9.1 μm^{-1} HTP obtained was found by fitting the average twisted angles.

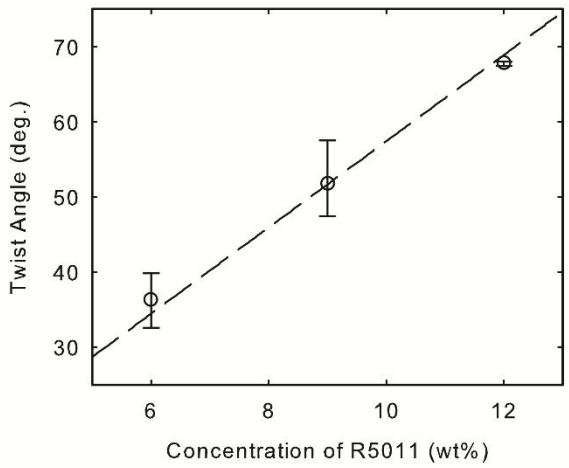

Figure S5. The twisted angle as a function of blending concentration of chiral dopant, R5011. The empty circles represent average values of twisted angles, and the dashed line represents fitted data using the above equation.

5. Mueller matrix analysis for the *g* value in PL and EL cases

When light propagates through a birefringent medium, its polarization state is easily described by the Stokes vectors. The transformation of the Stokes vectors of a beam of radiation is expressed by the Mueller matrix.[8] To calculate the g value using the Mueller matrix analysis, we take the assumption used in evaluating the twisted angle. We assume that the F8BT layer is continuously and uniformly twisted in the film and divide it into 10 sublayers of 10 nm.[9]

In the PL case, the UV light was absorbed, and the visible light was emitted at the *j*-th sublayer. The emitted light passes through the twisted birefringent medium from the *j*-th sublayer to the 10th sublayer and can be written in the form;

$$\mathbf{S}_{jo} = \left(\prod_{i=j}^{10} \mathbf{M}(\Gamma, \theta_i) \right) \mathbf{S}_j,$$

where $\mathbf{S}_j$ and $\mathbf{S}_{jo}$ depict the Stokes vector of the emitted light at the *j*-th sublayer and that of the outgoing light, respectively, and $\mathbf{M}(\Gamma, \theta_i)$ represents the Mueller matrix for the *i*-th sublayer with a phase retardation Γ. The Mueller matrix $\mathbf{M}(\Gamma, \theta_i)$ is represented as follows:

$$\mathbf{M}(\Gamma, \theta_i) = \begin{pmatrix} 1 & 0 & 0 & 0 \\ 0 & \cos(2\theta_i) & -\sin(2\theta_i) & 0 \\ 0 & \sin(2\theta_i) & \cos(2\theta_i) & 0 \\ 0 & 0 & 0 & 1 \end{pmatrix} \begin{pmatrix} 1 & 0 & 0 & 0 \\ 0 & 1 & 0 & 0 \\ 0 & 0 & \cos(\Gamma) & -\sin(\Gamma) \\ 0 & 0 & \sin(\Gamma) & \cos(\Gamma) \end{pmatrix} \begin{pmatrix} 1 & 0 & 0 & 0 \\ 0 & \cos(2\theta_i) & \sin(2\theta_i) & 0 \\ 0 & -\sin(2\theta_i) & \cos(2\theta_i) & 0 \\ 0 & 0 & 0 & 1 \end{pmatrix}$$

$$= \begin{pmatrix} 1 & 0 & 0 & 0 \\ 0 & \cos^2(2\theta_i) + \sin^2(2\theta_i)\cos(\Gamma) & \cos(2\theta_i)\sin(2\theta_i)\{1 - \cos(\Gamma)\} & \sin(2\theta_i)\sin(\Gamma) \\ 0 & \cos(2\theta_i)\sin(2\theta_i)\{1 - \cos(\Gamma)\} & \sin^2(2\theta_i) + \cos^2(2\theta_i)\cos(\Gamma) & -\cos(2\theta_i)\sin(\Gamma) \\ 0 & -\sin(2\theta_i)\sin(\Gamma) & \cos(2\theta_i)\sin(\Gamma) & \cos(\Gamma) \end{pmatrix}.$$

In the EL case, it is important to consider the recombination zone since, unlike for PL, light is emitted only in the recombination zone in both directions toward the anode and the cathode. We assumed that linearly polarized light is emitted at the *j*-th sublayer when electron and hole are recombined at the uniformly aligned *j*-th sublayer. The emitted light is propagated with the same probability toward the anode and the cathode. Therefore, the emitted light passes through the twisted birefringent medium from the *j*-th sublayer to the 10th sublayer, and the emitted light toward the anode and the cathode can be written as follows:

$$\mathbf{S}_{anode} = \left(\prod_{i=j}^{10} \mathbf{M}(\Gamma, \theta_i) \right) \mathbf{S}_j,$$

$$\mathbf{S}_{cathode} = \left(\prod_{i=0}^{10} \mathbf{M}(\Gamma, \theta_i) \right) \left(\prod_{i=0}^{j} \mathbf{M}(\Gamma, \theta_i) \right)^T \mathbf{S}_j.$$

Here, $\mathbf{S}_{anode}$ and $\mathbf{S}_{cathode}$ depict the Stokes vectors of the outgoing light to the anode and the cathode, respectively. The Mueller matrix for the reverse direction of light can be expressed using transposition of the matrix. Therefore, $\mathbf{S}_{cathode}$ is calculated by multiplying the matrix representing the medium experienced by the *j*-th sublayer with the matrix representing the medium experienced by the cathode and the reflected light from the cathode.

By the definition of the Stokes parameters, intensity I_L of the left-handed circular polarization is $(S_0 + S_3)/2$, and the intensity I_R of the right-handed circular polarization is $(S_0 - S_3)/2$. Moreover, using the definition of the g value, $g_{ideal} = -2(S_3/S_0)$. In the PL case, we assume that the light was emitted with the same probability at all sublayers. Therefore, the final g_{ideal} was calculated by averaging over all $\mathbf{S}_{jo}$. Using all measured parameters such as total twisted angle, total thickness, birefringence, and the degree of polarization, the g value can be calculated as shown in Fig. 4. In the EL case, we assume that the light emitted at a certain position within the emitting layer propagates toward anode or cathode with the same probability. Therefore, the final g_{ideal} was averaged over both propagating lights toward the anode and cathode. Using all measured parameters such as emitting position (*j*-th sublayer), total twisted angle, total thickness, birefringence, and degree of polarization, the g value can be calculated as shown in Fig. 4.

6. Evaluating g_{PL} and g_{EL} from CPPL and CPEL spectra

For various contact distances, the g_{PL} values were determined at 546 nm from the CPPL spectra. Figs. S6 and 7 show the CPPL spectra of the F8BT PL samples prepared with 6 wt% and 9 wt% of R5011, respectively. Order parameters according to the contact distance was evaluated from Fig. 3(d) and the corresponding g_{PL} values with respect to order parameter were shown in Fig. 4(c).

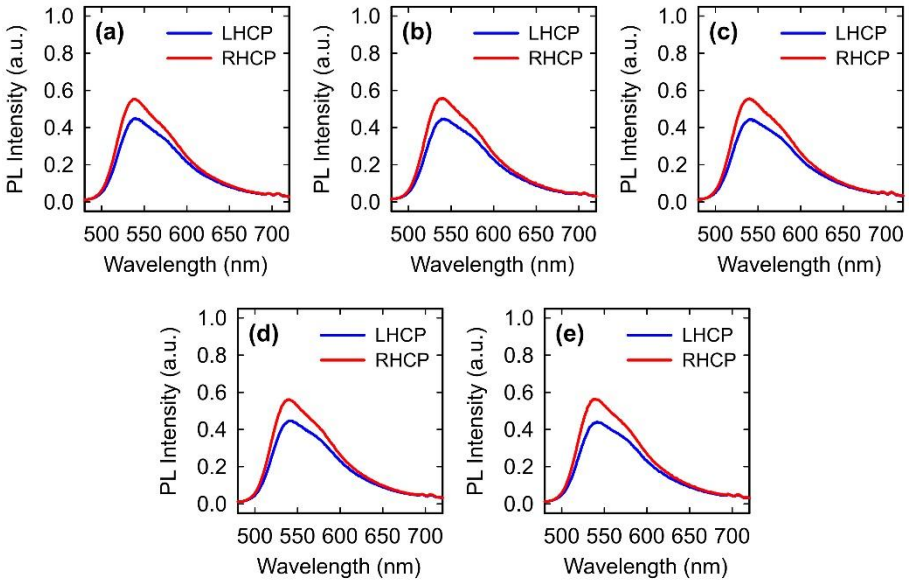

Figure S6. The CPPL spectra of the 100-nm-thick F8BT films with 6 wt% of R5011 under LH and RH circular polarisers with contact distances of (a) 0, (b) 10, (c) 20, (d) 30, and (e) 40 μm, respectively. Here, the determined g_{PL} values at 546 nm were evaluated to be (a) 0.197, (b) 0.206, (c) 0.212, (d) 0.219, and (e) 0.232.

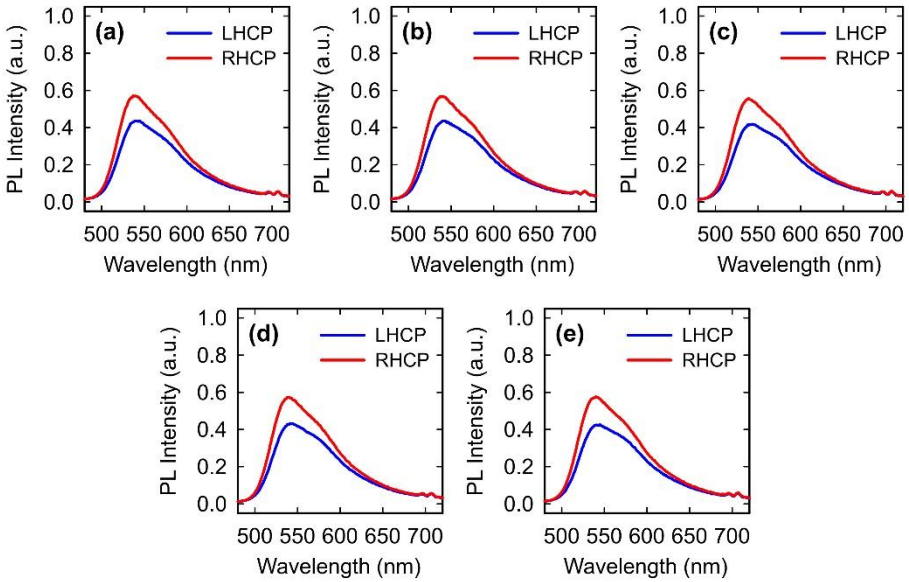

Figure S7. The CPPL spectra of the 100-nm-thick F8BT films with 9 wt% of R5011 under LH and RH circular polarisers with contact distances of (a) 0, (b) 10, (c) 20, (d) 30, and (e) 40 μm, respectively. Here, the determined g_{PL} values at 546 nm were evaluated to be (a) 0.242, (b) 0.249, (c) 0.258, (d) 0.267, and (e) 0.281.

Similarly, the g_{EL} values were also determined at 546 nm from the CPEL spectra. Figs. S8–10 show the CPEL spectra of the F8BT EL samples prepared with 6 wt%, 9 wt%, and 12 wt% of R5011, respectively. Order parameters according to the contact distance was evaluated from Fig. 3(d) and the corresponding g_{EL} values with respect to order parameter were shown in Fig. 4(d).

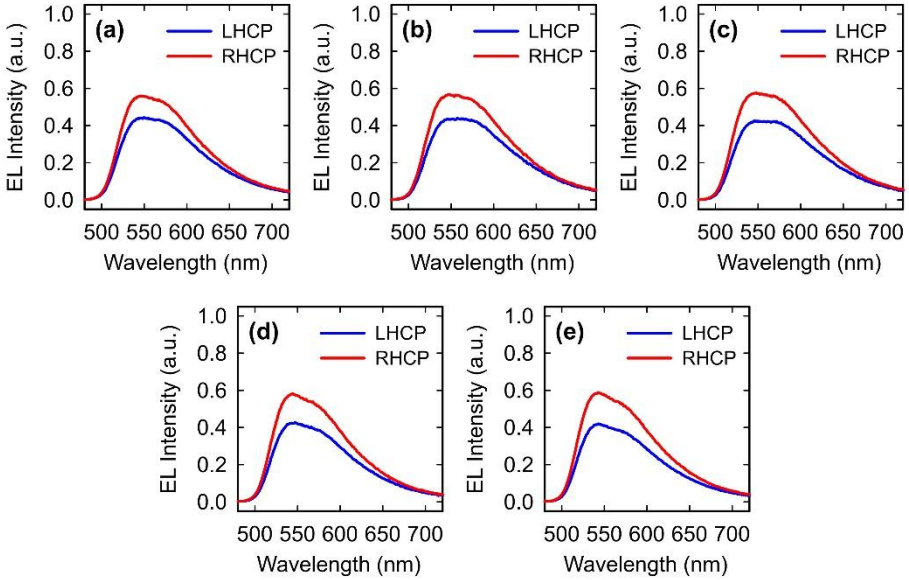

Figure S8. The CPEL spectra of the 100-nm-thick F8BT films with 6 wt% of R5011 under LH and RH circular polarisers with contact distances of (a) 0, (b) 10, (c) 20, (d) 30, and (e) 40 μm, respectively. Here, the determined g_{EL} values at 546 nm were evaluated to be (a) 0.237, (b) 0.261, (c) 0.296, (d) 0.311, and (e) 0.337.

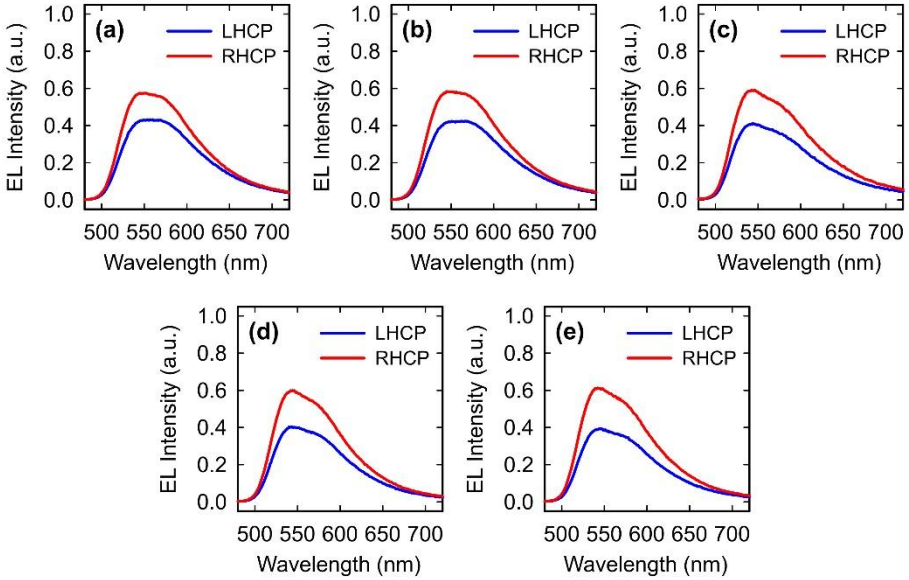

Figure S9. The CPEL spectra of the 100-nm-thick F8BT films with 9 wt% of R5011 under LH and RH circular polarisers with contact distances of (a) 0, (b) 10, (c) 20, (d) 30, and (e) 40 μm, respectively. Here, the determined g_{EL} values at 546 nm were evaluated to be (a) 0.292, (b) 0.329, (c) 0.366, (d) 0.394, and (e) 0.422.

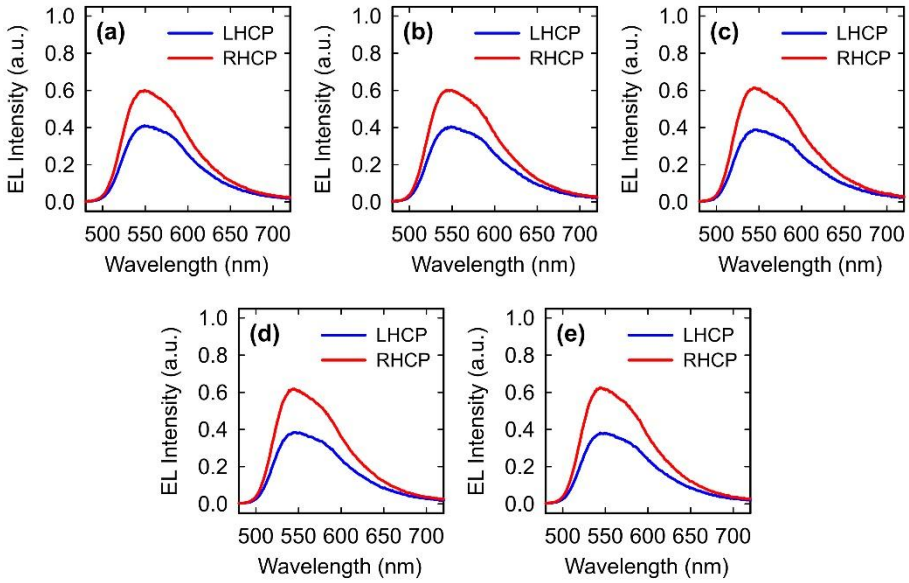

Figure S10. The CPEL spectra of the 100-nm-thick F8BT films with 12 wt% of R5011 under LH and RH circular polarisers with contact distances of (a) 0, (b) 10, (c) 20, (d) 30, and (e) 40 μm, respectively. Here, the determined g_{EL} values at 546 nm were evaluated to be (a) 0.378, (b) 0.402, (c) 0.445, (d) 0.463, and (e) 0.490.

We also measured circular dichroism (CD) of the F8BT layer with chiral dopant to confirm that the measured *g* value was originated from the twist structure. There is little difference in absorption spectra in LH and RH circular polarizers as shown in Fig. S11. Such CD was very small to produce the *g* value.

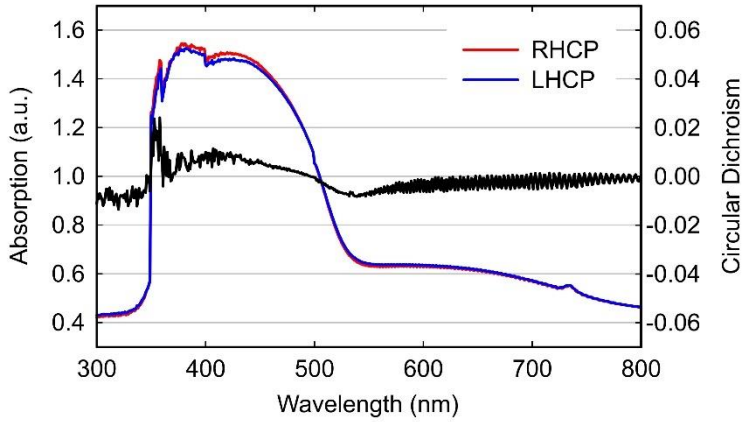

Figure S11. Absorption spectra of the twisted F8BT layer under LH and RH circular polarizers and the resulting CD.

7. IVL characteristics

The current density(J)-voltage(V)-luminance(L) characteristics of the F8BT with 6 wt% R5011 prepared with contact distance of 40 μm was measured by using a spectroradiometer, a programmable power supply, and multi-meter. As shown in Figure S12, the maximum efficiency was measured to be 0.38 cd/A, which is much lower than that in commercialized emission materials. It should be noted that the efficiency strongly depends on the material purity, fabrication environments, and so on.

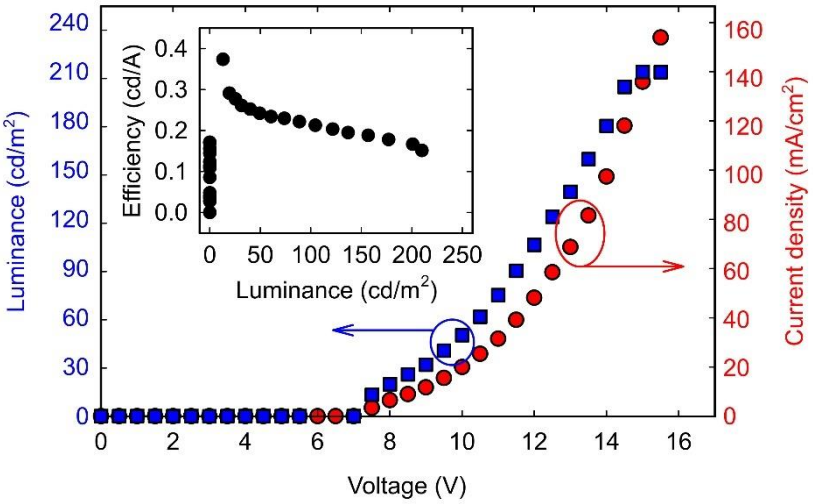

Figure S12. IVL characteristics of the F8BT with 6 wt% R5011 prepared with contact distance of 40 μm.

References

1 J. C. D. Faria, A. J. Campbell and M. A. McLachlan, *Adv. Funct. Mater.*, 2015, 25, 4657-4663.
2 H. Tanaka, H. Kajii and Y. Ohmori, *Syn. Metals*, 2015, **203**, 10-15.
3 J.-H. Lee, C.-J. Yu and S.-D. Lee, *Mol. Cryst. Liq. Cryst.*, 1998, **321**, 317-322.
4 I. M. Ward, *Structure and properties of oriented polymers*, Applied Science Publishers Ltd, London, 1975.
5 J.-H. Jung, D.-M. Lee, J.-H. Kim and C.-J. Yu, *J. Mater. Chem. C*, 2018, **6**, 726-730.
6 Y. Zhou, Z. He and S Sato, *Jpn. J. Appl. Phys.*, 1997, **36**, 2760–2764.
7 P.-G. De Gennes and J. Prost, *The physics of liquid crystals*, Oxford university press, Oxford, 1993.
8 A. A. Kokhanovsky, *Light scattering reviews 4: Single light scattering and radiative transfer*. Springer Science & Business Media, Chichester, 2009.
9 D. S. Kliger, J. W. Lewis and C. E. Randall, in *Polarized Light in Optics and Spectroscopy*, Academic Press, Inc., San Diego, 1990, ch.2.